Flow visualization through spacer filled channels by computational fluid dynamics I. Pressure drop and shear rate calculations for flat sheet geometry

Karode, Sandeep K.; Kumar, Ashwani

Publisher's version / Version de l'éditeur:
https://doi.org/10.1016/S0376-7388(01)00494-X
Journal of Membrane Science, 193, October 1, pp. 69-84, 2001

ELSEVIER

Journal of Membrane Science 193 (2001) 69–84

journal of MEMBRANE SCIENCE

www.elsevier.com/locate/memsci

Flow visualization through spacer filled channels by computational fluid dynamics I. Pressure drop and shear rate calculations for flat sheet geometry☆

Sandeep K. Karode, Ashwani Kumar*

National Research Council of Canada, Institute for Chemical Process and Environmental Technology, Montreal Road Campus, Ottawa, ON, Canada K1A 0R6

Received 22 March 2001; received in revised form 2 May 2001; accepted 2 May 2001

Abstract

Computational fluid dynamics (CFD) simulations were carried out for fluid flow through rectangular channels filled with several commercially available spacers for membrane modules. Simulation results were compared with literature experimental data. Excellent agreement was found between the experimentally determined dependence of the total drag coefficient on the Reynolds number and the CFD simulations in this work. Analysis of the flow structure through spacer filled channels revealed that bulk of the fluid does not change direction at each mesh as suggested previously in the literature, but that the bulk fluid flows parallel to the spacer filaments. The pressure drop through the channel was found to be largely governed by a loss of fluid momentum caused due to an almost abrupt change in the direction of the velocity vectors across a thin transition plane corresponding to the plane of intersection of the spacer filaments. It was observed that spacers with equal filament diameters usually result in a higher pressure drop across the channel and such symmetric spacers also result in a more uniform shear rate at the top and bottom faces of the test cell. Asymmetric spacers (spacers with unequal filament diameters) resulted in lower pressure drop and also induced unequal shear rate on the top and bottom faces of the test cell. Such unequal shear rates at the top and bottom faces would be expected to have an adverse impact on the membrane module performance because of different mass transfer characteristics for adjacent membrane leaves. It was found that a higher overall bulk turbulent flow would not necessarily result in higher shear rates at the top and bottom faces. © 2001 Published by Elsevier Science B.V.

Keywords: Computational fluid dynamics; Spacer; Flat sheet; Membrane; Fluid flow

1. Introduction

Spiral wound membrane modules is one of the most common membrane configurations in field application of membrane technology. Successful field operation requires a combination of various factors, the two most important being high performance membranes and modules that provide higher shear rates at the membrane surface. Net-type spacers are an essential feature in commercially available spiral wound modules. Such spacers play a dual role, first, keeping adjacent membrane leaves apart so as to form a feed channel and, second, promoting the mixing between the bulk of the fluid and the fluid element adjacent to the membrane surface so as to keep membrane

☆ NRCC No. : 44364

* Corresponding author. Tel.: +1-613-998-0498; fax: +1-613-941-2529.
E-mail address: ashwani.kumar@nrc.ca (A. Kumar).

0376-7388/01/$ – see front matter © 2001 Published by Elsevier Science B.V.
PII: S0376-7388(01)00494-X

Nomenclature

A	characteristic constant for a given spacer and it's orientation (defined in Eq. (6))
C_d	total drag coefficient (defined in Eq. (6))
d_f	diameter of spacer filament (m)
d_h	hydraulic diameter (m)
h_{sp}	height of spacer (m)
l_f	distance between parallel filaments measured perpendicular to the filament (m)
L	length of test cell (m)
P	pressure (Pa)
Re	Reynolds number (defined in Eq. (7))
u	X-component of velocity (m/s)
u_0	inlet velocity into test cell (m/s)
	Y-component of velocity (m/s)
	Z-component of velocity (m/s)
x	X-direction corresponding to the direction of bulk flow along channel axis
y	Y-direction corresponding to the width of the test cell
z	Z-direction corresponding to the height of the spacer (and test cell)

Greek letters

	spacer porosity
	fluid viscosity (Pa s)
	hydrodynamic angle (°)
	fluid density (kg/m^3)

surface relatively clean. Efficient membrane module performance depends on the efficacy of the spacers to increase mass transport away from the membrane surface so as to reduce concentration polarization by increasing the shear rate at the membrane surface [1].

Net-type spacers of expanded aluminum were first used by Glatzel and Tomaz [2] to study heat transfer and pressure drop. They reported that changing the orientation of the spacer had an effect on the heat transfer and pressure drop across the spacer filled channel, but did not analyze their results in detail. Following this, pressure drop and mass transfer in spacer filled channels (using expanded aluminum and corrugated PVC sheets) was studied by Hicks [3] by an electrochemical reaction. He identified that the angle between the channel axis and the spacer filament (or strand) to be an important parameter governing pressure drop.

Schock and Miquel [4] studied reverse osmosis (RO) in spacer filled channels. They claimed that mass transport could be described independently of the type of spacer by a turbulent flow correlation with a power of the Reynolds number (Re) of 0.875. Da Costa and co-workers [1,5,6] systematically studied pressure drop and flux through membranes in flat sheet geometry for various commercially available spacers in the feed channel. They used an HFK-131 polysulfone membrane with a nominal molecular weight cut-off of 5000 Da (Koch Membranes Inc.) and DextranT-300/DextranT-500 as the solute. They measured flux and pressure drop in a rectangular test cell for a range of bulk cross-flow rates. The membrane was the bottom face of the test cell. They defined an important spacer characteristic, namely, the hydrodynamic angle, which describes the change in direction of the fluid as it flows in the channel. They concluded that mass transfer could be described by a laminar flow-type correlation while pressure drop was best described by a turbulent type correlation.

Da Costa et al. [5] also proposed a mathematical model to describe pressure drop for steady-state fluid flow across spacer filled channels by including viscous drag on the channel walls and the spacer, form drag of the spacer and kinetic losses due to directional flow change. The primary focus of this work is to estimate overall pressure drop for fluid flow across spacer filled channels by rigorously solving the steady-state Navier–Stokes equations in a 3D rectangular flow domain. As will be shown later in this manuscript, Da Costa et al. [5] were quite successful in determining overall channel pressure drop by specifically accounting for various pressure drop terms. However, based on the relative contribution of the above terms to the overall pressure drop they incorrectly concluded that, "a large proportion of the fluid follows a zigzag path, changing direction at each mesh" [5].

In this work, we report results from a computational fluid dynamics (CFD) study to visualize the steady-state fluid flow structure through spacer filled channels in flat sheet form. CFD simulations for these commercially available spacers used by Da Costa and co-workers [1,5,6] give an insight on the actual fluid

flow structure in flow across spacer filled channels. It is shown that the bulk of the fluid does not change direction at each mesh, but that the overall flow path is a function of the spacer filament dimensions. Most of the pressure drop is due to the change in the direction of the velocity vector across a thin transition region corresponding to the plane of intersection of the spacer filaments. Average shear rates at the top and bottom face of the flow cell are also reported.

2. The test cell

We model the test cell used by Da Costa and co-workers [1,5,6] in their studies on flux optimization and pressure drop modeling in spacer filled flat sheet membranes using various spacers. The height of the rectangular channel corresponded to the spacer thickness. In this work, the test cell dimensions were 25 mm wide, 35 mm long (Da Costa et al.'s cell was 280 mm long). The pressure drop for a cell length of 280 mm was calculated from the simulation results by assuming that the change in pressure per unit length (i.e. the pressure gradient) was constant. The spacer filaments were idealized as cylindrical rods oriented at appropriate angles to the channel axis. To maintain consistency and to facilitate comparison, the nomenclature of the spacers used by Da Costa et al. [5] has been kept the same. The geometric characteristics of the various spacers studied in this work are given in Table 1. For spacers with unequal filament diameters, the spacer filament diameter and inter-filament spacing for thick filaments are given in parentheses in Table 1.

3. Governing equations

The governing equations for steady-state fluid flow in a rectangular geometry are the equation of continuity and the three equations of motion [7]:

$$\frac{}{} + \frac{}{} + \frac{}{} = 0 \tag{1}$$

$$\left(\frac{}{} + \frac{}{} + \frac{}{} \right) = -\frac{}{} + \left(\frac{^2}{_2} + \frac{^2}{_2} + \frac{^2}{_2} \right) \tag{2}$$

Table 1
Geometric characteristics of spacers

Spacer name	h_{sp} ($\times 10^3$ m)	d_f ($\times 10^3$ m)	l_f ($\times 10^3$ m)		(°)	d_h[a] ($\times 10^3$ m)
Conwed-1[b]	2.01	1.03	2.17	0.618	90	0.997
Conwed-2[c]	2.01	1.03	2.17	0.618	0	0.997
NALTEX-56[d]	1.11	0.55	4.3	0.880	56	1.316
NALTEX-124[e]	1.11	0.55	4.3	0.880	124	1.316
NALTEX-51-1[f]	1.17	0.5 (0.7)	2.89 (5.37)	0.846	51	1.226
NALTEX-129[g]	1.17	0.5 (0.7)	2.89 (5.37)	0.846	129	1.226
NALTEX-51-2[h]	1.17	0.5 (0.7)	2.89 (5.37)	0.846	0	1.226
NALTEX-51-3[i]	1.17	0.5 (0.7)	2.89 (5.37)	0.846	0	1.226
UF1[j]	1.68	0.76 (1.07)	4.06 (5.3)	0.763	0	1.375
UF4[k]	1.68	0.76 (1.07)	4.06 (5.3)	0.763	45	1.375

[a] As defined by Schock and Miquel [4].
[b] Bottom filament 45° to channel axis (anticlockwise); top filament 45° to channel axis (clockwise).
[c] Conwed-1 spacer rotated by 90° (bottom filaments parallel to channel axis).
[d] Bottom filament 28° to channel axis (anticlockwise); top filament 28° to channel axis (clockwise).
[e] NALTEX-56 spacer rotated by 90°.
[f] Bottom filament (thick) 30° to channel axis (anticlockwise); top filament (thin) 21° to channel axis (clockwise).
[g] NALTEX-51-1 spacer rotated by 82°.
[h] NALTEX-51-1 spacer rotated by 160° (top (thin) filaments parallel to channel axis).
[i] NALTEX-51-1 spacer rotated by 30° (bottom (thick) filaments parallel to channel axis).
[j] Bottom (thick) filaments parallel to channel axis; top (thin) filaments 45° to channel axis (anticlockwise).
[k] UF1 spacer rotated by 20°.

$$\left(\frac{}{} + \frac{}{} + \frac{}{} \right) = -\frac{}{} + \left(\frac{^2}{^2} + \frac{^2}{^2} + \frac{^2}{^2} \right) \quad (3)$$

$$\left(\frac{}{} + \frac{}{} + \frac{}{} \right) = -\frac{}{} + \left(\frac{^2}{^2} + \frac{^2}{^2} + \frac{^2}{^2} \right) \quad (4)$$

where u, , denote the x, y, z components of the velocity, respectively; is the fluid density (water, in this case) and the viscosity of the fluid. P denotes the fluid pressure.

The x-coordinate denotes the direction of bulk flow (channel axis) with $= 0$ corresponding to the inlet and $=$ corresponding to the outlet ($= 0.035$ m in this case); $= 0$ corresponds to the bottom face of the cell (which was the membrane in Da Costa et al.'s work [5]) and $= _{sp}$ corresponds to the top face. The y-coordinate is along the width of the cell ($=$ $= 0.025$ m in this case).

The boundary conditions for Eqs. (1)–(4) are

$$= 0 \quad = _0; \quad = 0; \quad = 0 \quad (5a)$$

$$= \quad = 0 \quad (5b)$$

$$= 0; \quad = \quad = \quad = \quad = 0 \quad (5c)$$

Additionally, the no-slip boundary condition is assumed to hold at all fluid–solid interfaces, i.e. at the bottom and top faces and at the surface of the spacer filaments.

Governing Eqs. (1)–(4) along with boundary conditions (Eq. (5a)–(5c)) are solved by the finite volume formulation of Patankar [8]. This method involves subdividing the flow cell into a number of finite volumes by generating a rectangular grid fitting the physical flow domain. A schematic of the test cell along with the spacer filaments and an X–Y grid slice is shown in Fig. 1. The volume of the spacer filaments is consequently discretized into a number of finite volume

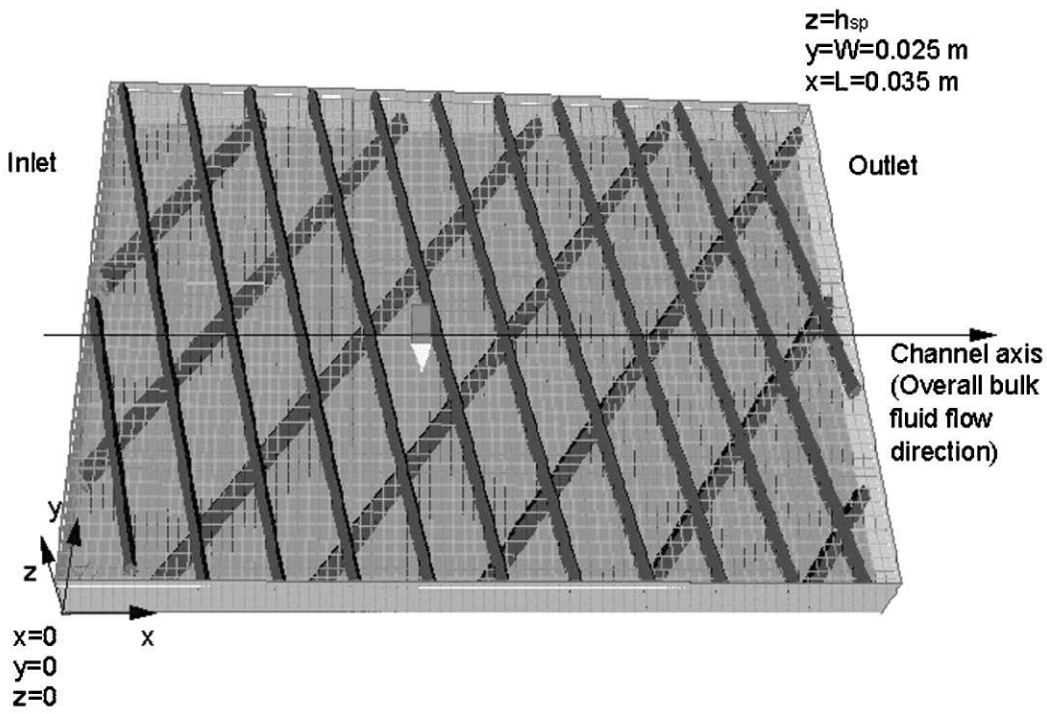

Fig. 1. Schematic of the rectangular test cell showing spacer filaments and a typical grid in the X–Y-plane.

cells corresponding to the rectangular grid. The finite volume cells corresponding to the spacer filaments have zero velocity at their faces (the no-slip boundary condition). The lower left corner of the rectangular test cell corresponds to the origin and the upper right corner corresponds to = , = , = sp. In our case, = 0 035 m and = 0 025 m. It must be mentioned here that, for spacers with non-equal filament diameters, the thicker filament was always kept adjacent to the bottom face (as done by Da Costa and co-workers [1,5,6] in their study).

The fluid flow Eqs. (1)–(4) are discretized using the hybrid scheme [8]. The staggered grid approach [8] is used to solve for the velocity and pressure components by the SIMPLE algorithm presented by Patankar [8]. A commercially available CFD routine, PHOENICS, was used to implement the fluid flow equations.

In this work, the test cell was divided into a number of finite elements by a x–y–z grid. Starting from a sparse grid, the grid was progressively refined by doubling the number of grids in any given direction till two successive simulations resulted in 0.1% variation between the velocity and pressure distribution in the computational space. Typically, a 160 × 80 × 40 grid was found to be suitable for all simulations in this work.

4. Results and discussion

Water was taken as the bulk fluid for all CFD simulations in this work. CFD simulations were run for inlet velocities ranging from 0.25 to 1.0 m/s that encompasses typical cross-flow velocities in commercial membrane modules. Following Da Costa et al. [5], we define a total drag coefficient, C_d and a Reynolds number, Re as follows:

$$_d = \frac{2 \quad Pd_h}{0 \quad ^2} = \frac{}{Re} \tag{6}$$

$$Re = \frac{_h \quad 0}{} \tag{7}$$

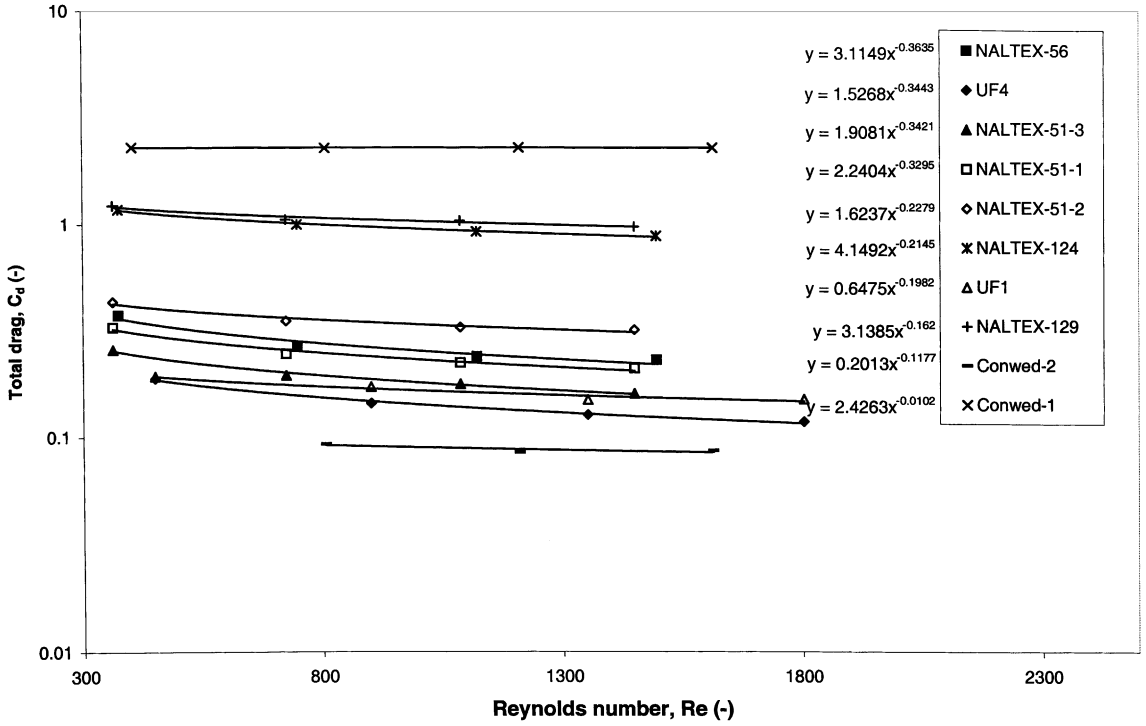

Fig. 2. Variation of the total drag as a function of Reynolds number for various spacers. The best-fit correlation for $_d =$ Re is shown beside the legend for each spacer.

Table 2
Hydrodynamic characteristics of spacers

Spacer	A		n	
	This work	Da Costa et al. [5]	This work	Da Costa et al. [5]
NALTEX-56	3.12	2.0	0.37	0.35
UF4	1.53	0.49	0.34	0.29
NALTEX-51-3	1.91	3.21	0.34	0.36
NALTEX-51-1	2.24	2.27	0.33	0.35
NALTEX-51-2	1.62	3.38	0.23	0.30
NALTEX-124	4.15	3.39	0.22	0.24
UF1	0.65	N.A.	0.20	N.A.
NALTEX-129	3.14	7.38	0.16	0.34
Conwed-2	0.20	1.19	0.12	0.16
Conwed-1	2.43	1.29	0.01	0.24

where A is a characteristic constant for a given spacer, P the channel pressure drop, L the length of the channel, u_0 the inlet velocity, d_h the hydraulic diameter of the spacer and the spacer porosity (see Table 1). The total drag coefficient is defined so as to incorporate the total pressure drop along the channel length.

Fig. 2 shows the total drag coefficient as a function of the Reynolds number for all the spacers studied in this work. Also shown on the figure is the best-fit curve corresponding to Eq. (6). The legend is arranged in decreasing magnitude of the Reynolds exponent n.

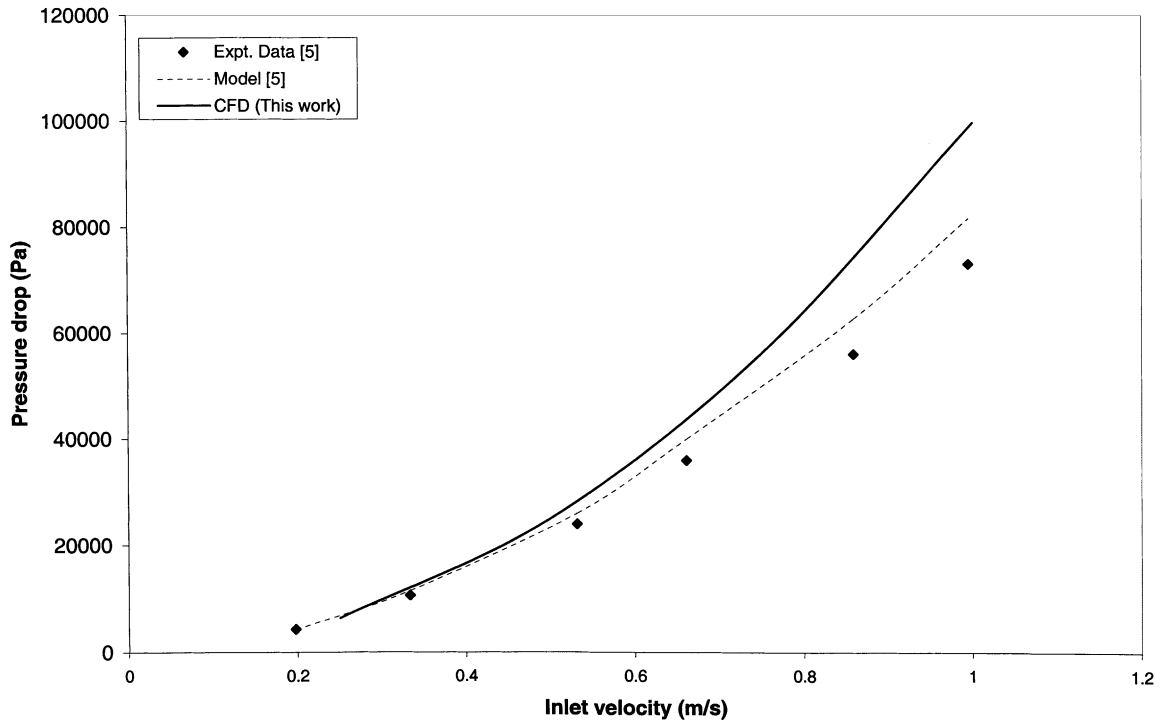

Fig. 3. Pressure drop across test cell of Da Costa et al. [5] as a function of inlet velocity for Conwed-1 spacer.

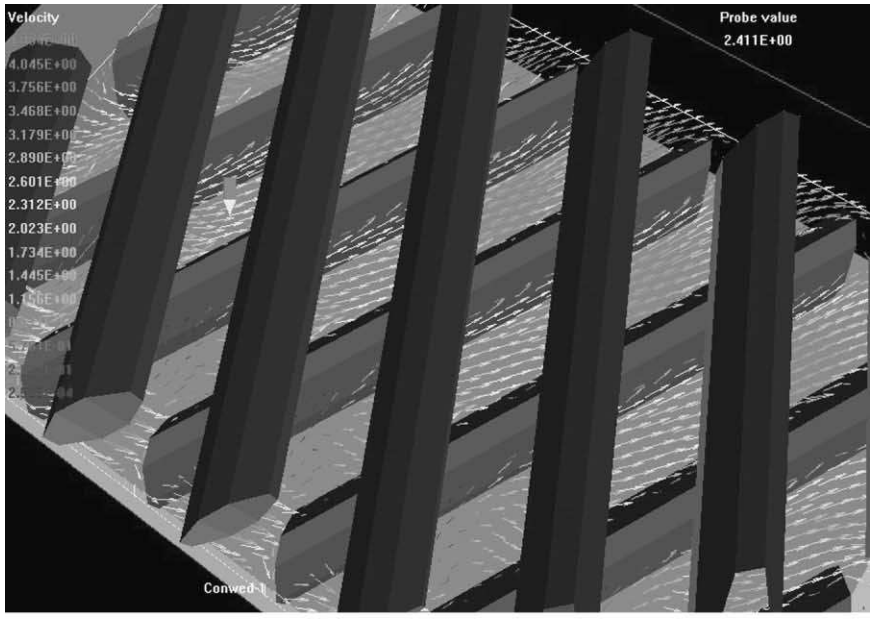

(a)

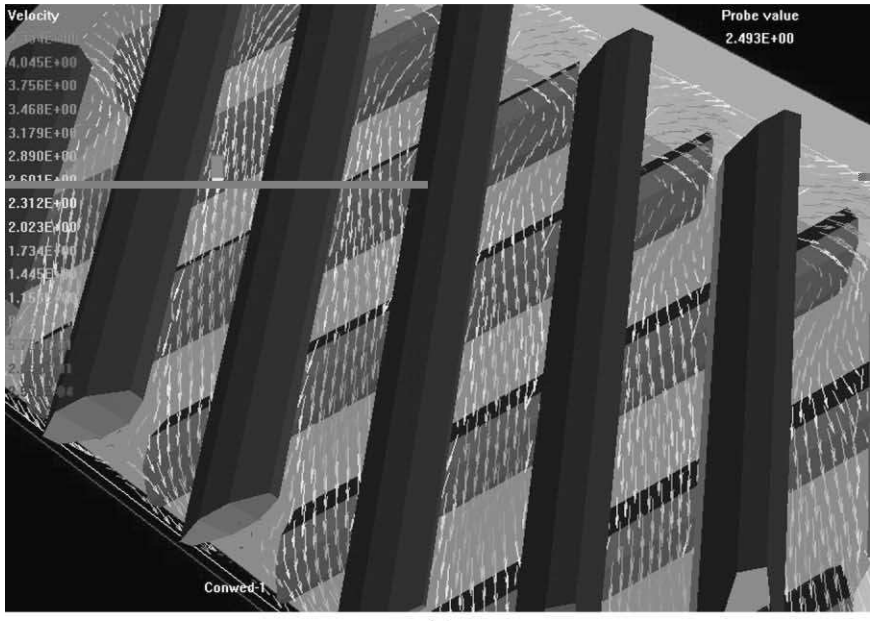

(b)

Fig. 4. (a) Velocity vectors at constant = 1 025 mm for Conwed-1 spacer for an inlet velocity of 1 m/s. (b) Velocity vectors at constant = 1 035 mm for Conwed-1 spacer for an inlet velocity of 1 m/s.

As discussed by Da Costa et al. [5], a lower value of n is indicative of higher degree of turbulence in the fluid flow. In their work, the spacers were characterized into three categories depending on the value of the Reynolds exponent n. A value of 0 18 was taken to indicate a high degree of turbulence [5]. A value between 0.18 and 0.25 indicated a transition regime while a value greater than 0.25 indicated predominantly laminar flow [5]. Fig. 2 predicts the macroscopic bulk flow to be highly turbulent for spacer Conwed-1 and least turbulent (or most laminar) for spacer NALTEX-56. Interestingly, as can be seen from Fig. 2, a higher degree of turbulence (deduced by the value of n) need not necessarily mean an increased total drag. For example, spacer Conwed-2 for which the flow appears to have a high degree of turbulence, has the least total drag, while the spacer NALTEX-129 in which the flow borders on a transition regime has one of the highest total drag coefficients. Table 2 lists the value of the parameter A and n from Eq. (6) for all spacers as calculated in this work and also the values experimentally measured by Da Costa et al. As can be seen from Table 2, there is good agreement in the Reynolds number dependence of C_d between the CFD simulation in this work and the experimentally measured dependence by Da Costa et al. [5] except for the case of NALTEX-129 and Conwed-1 spacers. The CDF simulations predict a marginally higher C_d than that measured by Da Costa et al. [5] probably because their data was masked by entrance and exit effects due to the positioning of their pressure sensing ports. However, it should be noted here that in rigorous terms, turbulence is an unsteady-state phenomenon. In this work, turbulence is taken to represent macroscopic mixing of fluid elements.

Fig. 3 shows the pressure drop across the test cell used by Da Costa et al. [5] as a function of inlet velocity for Conwed-1 spacer as predicted by the CFD

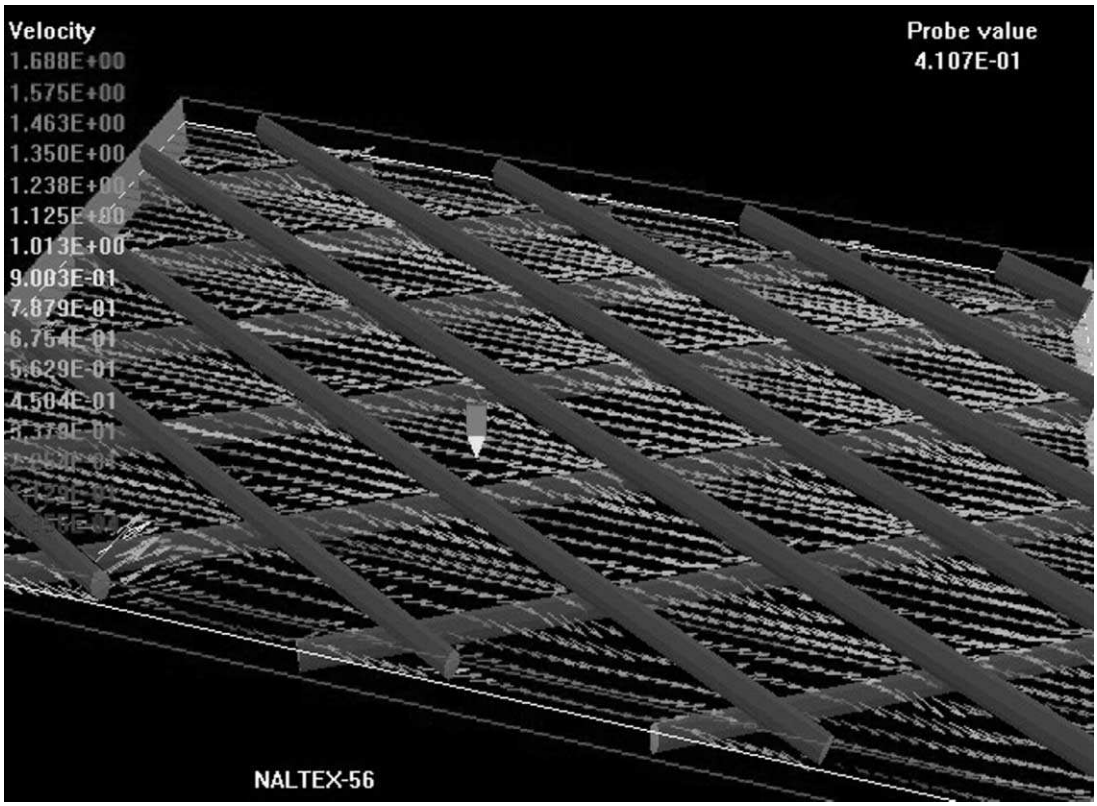

Fig. 5. Velocity vectors at constant = 0 55 mm for NALTEX-56 spacer for an inlet velocity of 1 m/s.

simulation in this work, experimental values reported by Da Costa et al. [5] and that predicted by the model proposed by Da Costa et al. [5]. As can be seen from Fig. 3, at low inlet velocities (0.5 m/s), where entrance and exit effects are relatively small, there is good agreement between the pressure drop predicted in this work and that experimentally measured by Da Costa et al. [5]. For higher inlet velocities, the CFD simulation in this work and the model proposed by Da Costa et al. over predict the pressure drop compared to that measured experimentally. This discrepancy could possibly be attributed to errors in measuring the pressure drop experimentally. Another possible reason of lower experimentally measured pressure drop is the non-ideality of the actual spacers. Real spacers have slightly undulating spacer filaments that could allow some fluid flow between the filament and the membrane. The idealized spacer in this work does not allow such short-circuiting of the fluid.

Da Costa et al. [5] concluded that most of the pressure drop is attributable to a large proportion of the fluid following a zigzag path, changing direction at each mesh. They show this schematically in Fig. 6 of their manuscript [5]. CFD simulations in this work do not support this conclusion. This can be seen from Fig. 4a and b for the Conwed-1 spacer. Fig. 4a and b show close up snapshots of the velocity vectors so as to show more detail. Filament diameter for Conwed-1 spacer is 1.03 mm (Table 1). For an inlet velocity of 1 m/s, Fig. 4a shows the velocity vectors at a plane corresponding to = 1 025 mm and Fig. 4b shows the velocity vectors at a plane corresponding to = 1 035 mm for the Conwed-1 spacer. Fig. 4a and b clearly show that bulk of the fluid indeed does not change direction at each mesh. Bulk fluid from = 0 to = 1 025 mm flows parallel to the spacer filament adjacent to the bottom face (Fig. 4a) while bulk fluid from = 1 035 to = 2 01 mm flows parallel to the spacer filament adjacent to the top face (Fig. 4b). Most of the pressure drop is due to momentum loss in the transition plane corresponding to intersection of the top and bottom spacer filaments (i.e. plane corresponding to = 1 03 mm). This was verified as follows.

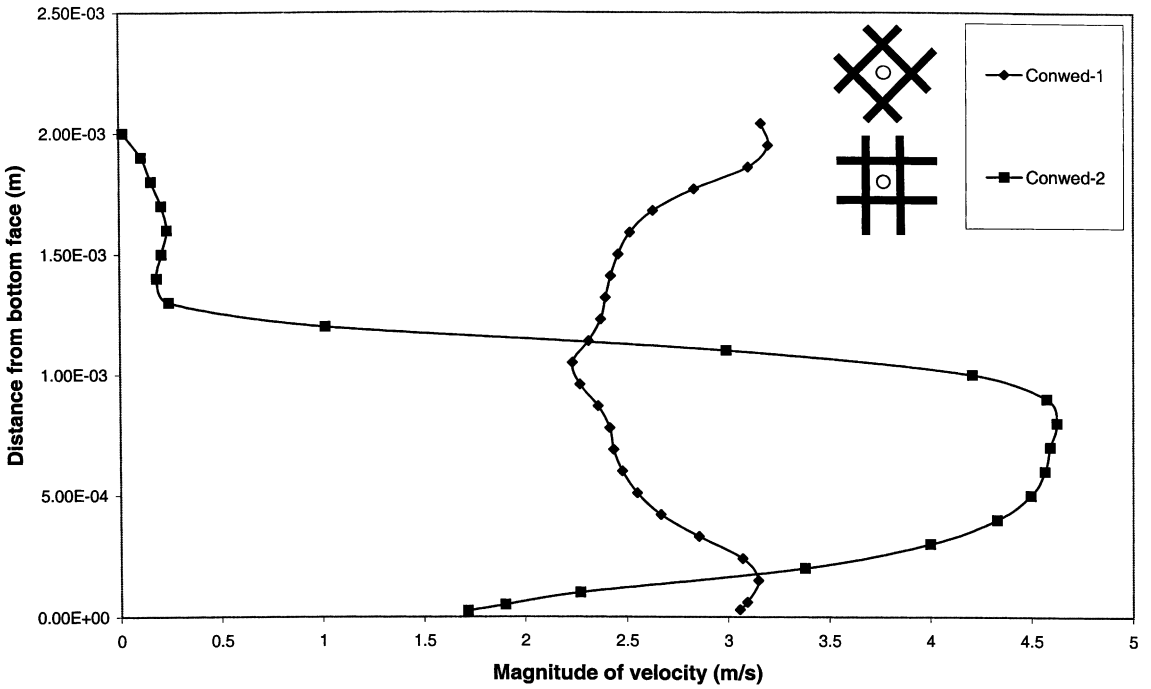

Fig. 6. Magnitude of the velocity (on the *X*-axis) as a function of the distance from the bottom face at an inlet velocity of 1 m/s. Spacers: Conwed-1, Conwed-2.

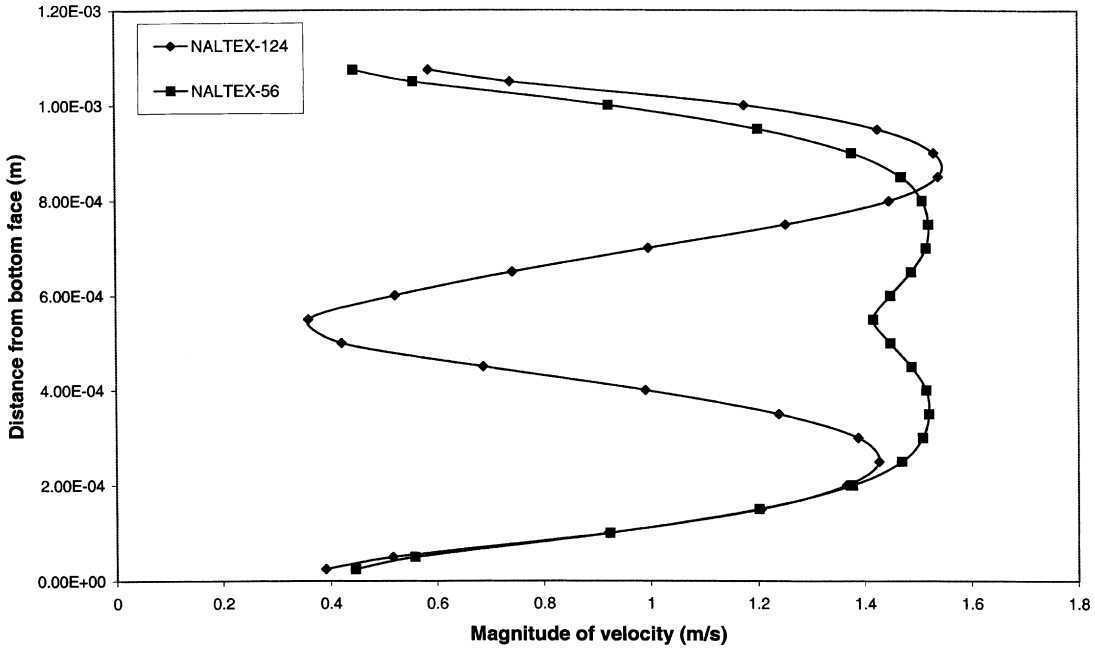

Fig. 7. Magnitude of the velocity (on the *X*-axis) as a function of the distance from the bottom face at an inlet velocity of 1 m/s. Spacers: NALTEX-56, NALTEX-124.

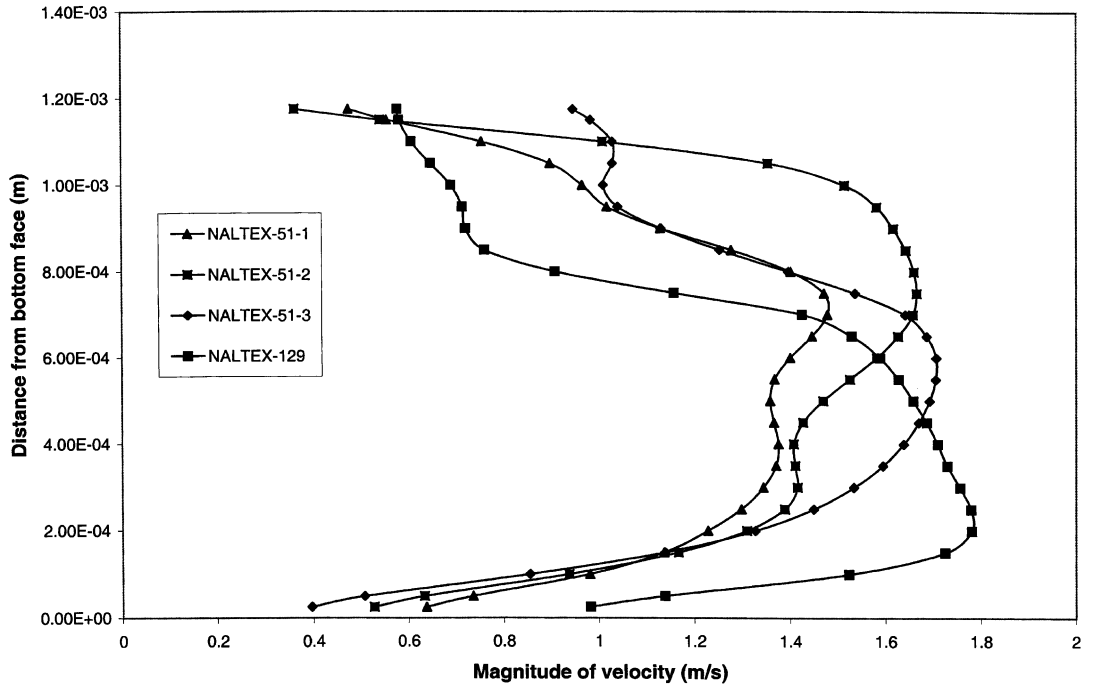

Fig. 8. Magnitude of the velocity (on the *X*-axis) as a function of the distance from the bottom face at an inlet velocity of 1 m/s. Spacers: NALTEX-51-1/2/3, NALTEX-129.

Simulations were run without the top layer of the spacer filaments in order to eliminate the abrupt rotation of the velocity vectors and to estimate the pressure drop corresponding to the form drag offered by the spacer filaments. Form drag for a single layer of spacer filaments resulted in only about (1/6)th of the total pressure drop. This shows that over and above the form drag, the abrupt rotation of the velocity vectors results in an additional energy loss that controls the overall pressure drop. This could also explain why the total drag coefficient is essentially independent of the flow rate.

The bulk fluid flow across the Conwed-1 spacer can now be deduced. The fluid predominantly flows parallel to the spacer filament axis till it encounters a vertical wall at the edge of the flow cell (= 0 or =). At the edge, the fluid from the top layer of the filaments turns downward into the channel created by the bottom layer of the spacers. This zigzag motion occurs only at the cell edge and not at each mesh intersection as suggested by Da Costa et al. [5].

Fig. 5 shows the velocity vectors at a constant z-plane at = 0 55 mm for the NALTEX-56 spacer at an inlet velocity of 1 m/s. The filament diameter for the NALTEX-56 spacer is 0.55 mm (Table 1). As can be seen from the figure, bulk of the fluid flows parallel to the channel axis and not along the spacer filaments as for the Conwed-1 spacer. This suggests that inter-filament spacing plays a dominant role in determining overall bulk fluid flow in spacer filled channels.

Fig. 6 shows the magnitude of the velocity vector on the X-axis as a function of z-distance from the bottom face for Conwed-1 and Conwed-2 spacers. Fig. 6 shows the velocity profile midway between the spacer filaments as shown in the sketch alongside the legend. As expected, the velocity profile for Conwed-1 is symmetric around = 1 03 mm. It can be seen

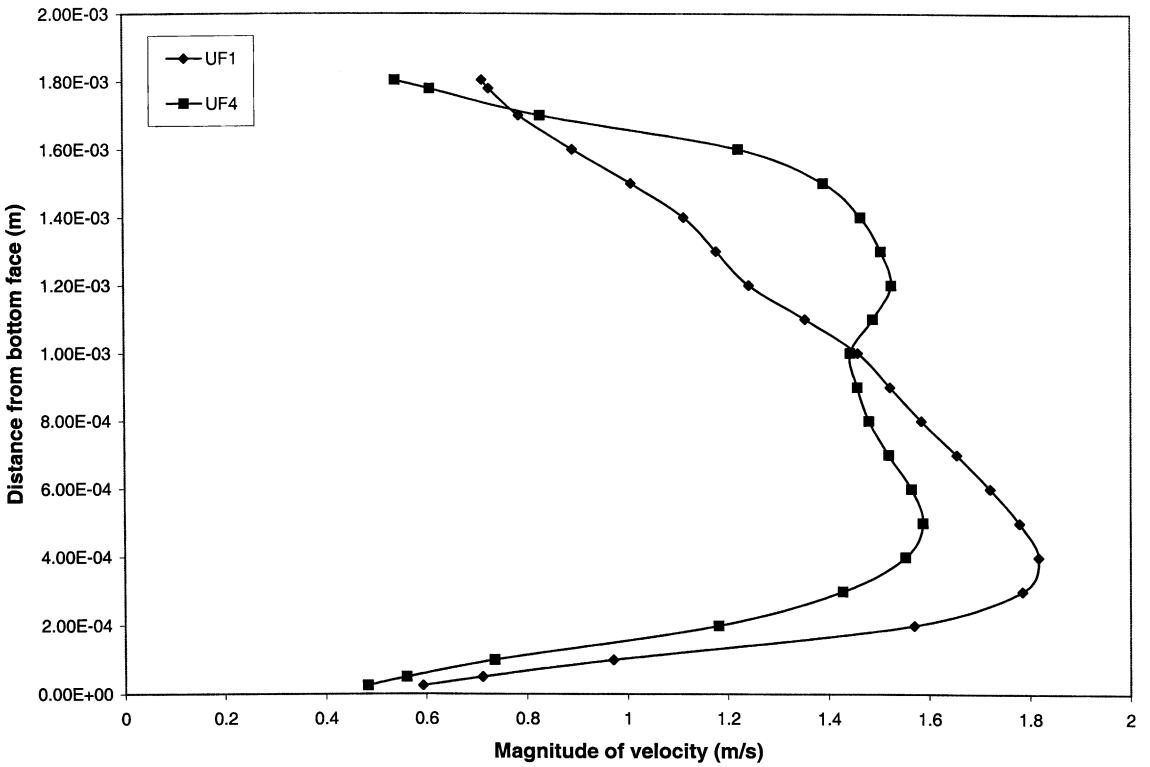

Fig. 9. Magnitude of the velocity (on the X-axis) as a function of the distance from the bottom face at an inlet velocity of 1 m/s. Spacers: UF1, UF4.

that the magnitude of the velocity (for the Conwed-1 spacer) goes through a minimum at $= 1\ 03$ mm due to a 90° change of direction in the transition plane. No such minimum is seen for the Conwed-2 spacer where the bulk of the flow takes the path of least resistance and flows along the bottom filaments. Consequently, there is a higher shear rate at the bottom face and a

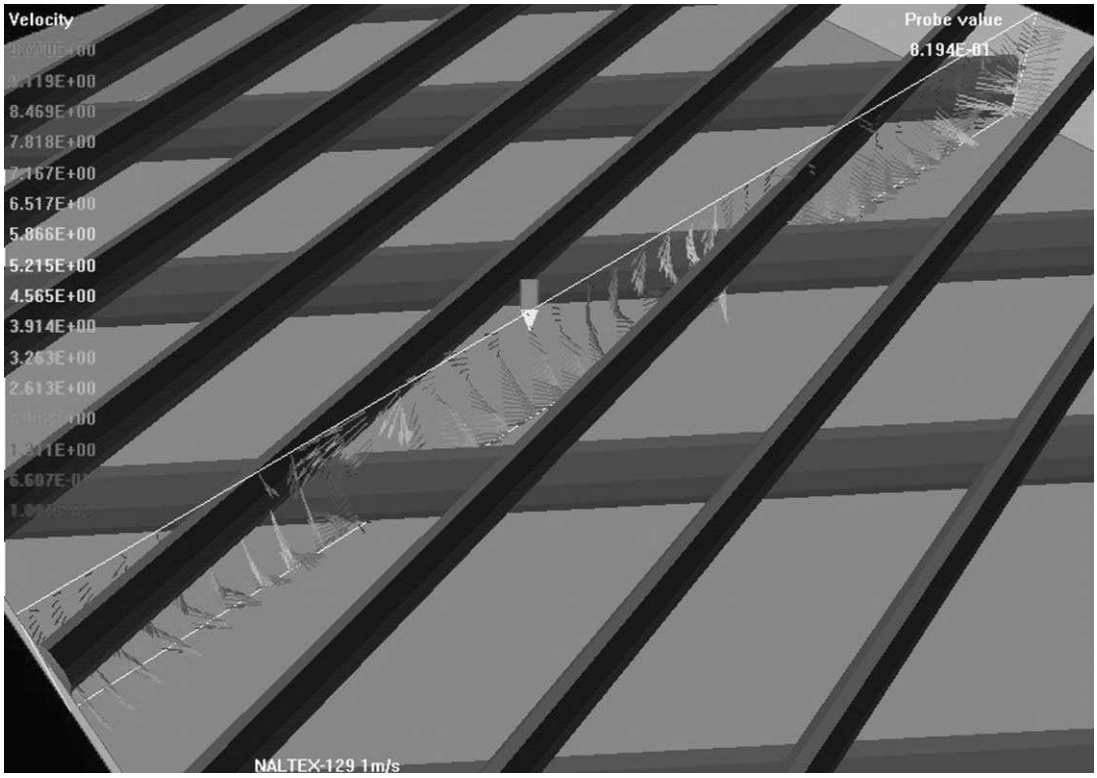

Fig. 11. Velocity vectors for constant x for an asymmetric NALTEX-129 spacer (inlet velocity = 1 m/s).

can be seen from this figure, for symmetric spacers like NALTEX-56 (124) and Conwed-1, the shear rate at the top and bottom faces is equal. Therefore, in such spacers, the membrane performance would be exactly identical whether it is placed on the bottom face or the top face.

For asymmetric spacers, there is a large variation in the shear rate on the top and bottom faces. The NALTEX-129 spacer forces majority of the fluid to flow along the thicker filament consequently causing a drastic reduction in the shear rate at the top face compared to the bottom face. NALTEX-51-1, however results in a more even shear rate between the top and bottom faces. Spacer UF1 for which the thick filament (adjacent to the bottom face) is parallel to the channel axis causes the majority of the fluid to flow along the bottom filament resulting in a high shear at the bottom face and a very low shear at the top face (similar to the Conwed-2 spacer). UF4, however has a more even shear rate at the top and bottom faces.

These spacers, when used in commercial spiral wound elements, would result in unequal shear rates at adjacent membrane faces resulting in non-uniform performance between the membrane leaves of the module. Such non-uniform operation of membrane leaves within a single spiral element is expected to eventually lead to accelerated deterioration of the overall membrane system. Symmetric spacers would not have this drawback.

In order to compare various spacers with respect to the shear rate, we need to define an "average" shear rate for a given spacer. As a first approximation, such an average could be defined as an arithmetic average of the shear rate at the top and bottom face. Fig. 13 shows the average shear rate for various spacers as a function of inlet velocity. As can be seen from the figure, at low inlet velocity, there is not much variation

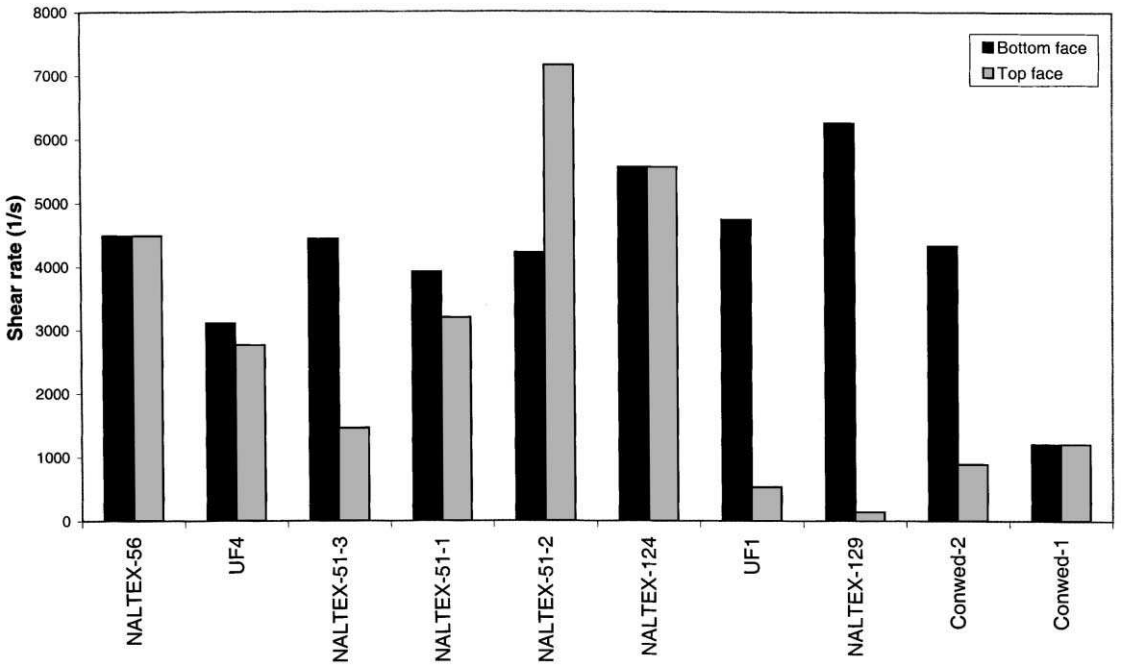

Fig. 12. Shear rate at the top and bottom faces for several spacers at an inlet velocity of 1 m/s.

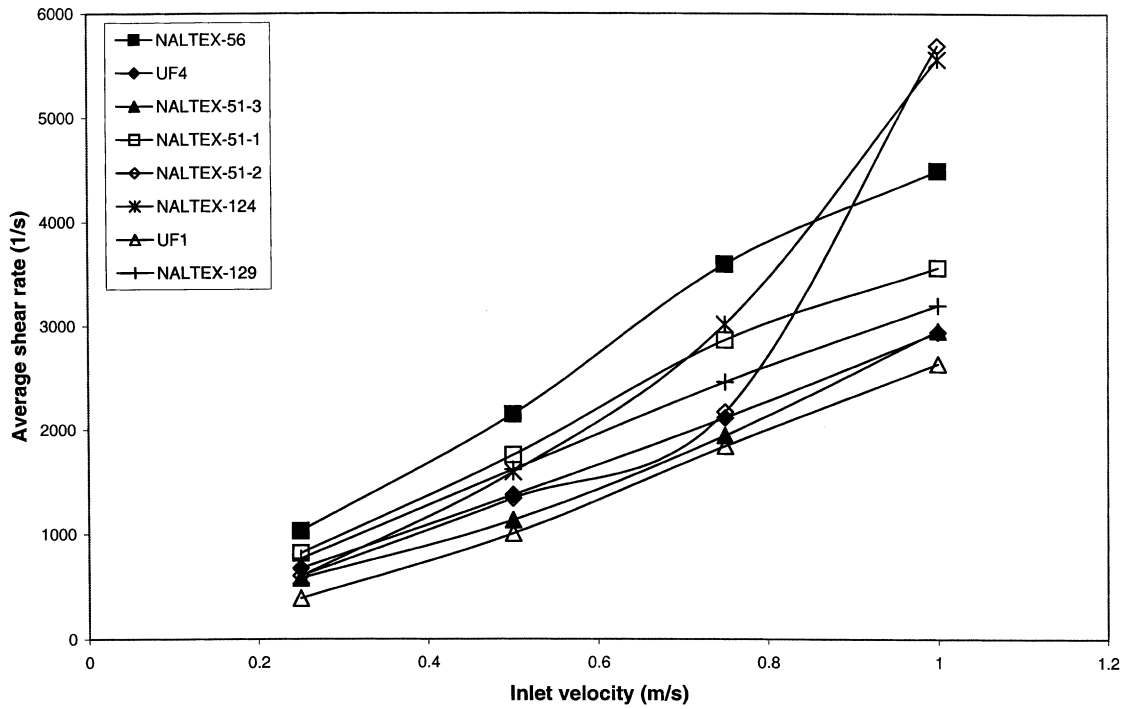

Fig. 13. Average shear rate as a function of inlet velocity for several spacers.

in the average shear rate for various spacers. However, spacers NALTEX-51-2 and NALTEX-124 result in a much higher shear rate compared to other spacers at high inlet velocity.

From Fig. 2, it can be seen that NALTEX-124 has a much higher total drag coefficient compared to NALTEX-51-2 which makes the NALTEX-51-2 spacer superior to other spacers in terms of both criteria, namely, lower total drag along with higher average shear.

5. Conclusions

Computational fluid dynamics simulations were run on several commercially available spacers for evaluating effectiveness of spacers in terms of the pressure drop and the average shear the fluid exerts on the top and bottom faces. Water was taken as the bulk fluid during all the simulations. The CFD program was benchmarked against literature experimental data for pressure drop through spacer filled channels in flat sheet geometry [5]. It was found that a $160 \times 80 \times 40$ x–y–z grid was suitable for engineering prediction of the pressure drop and shear rate.

The CFD simulations were in good agreement with reported experimental data for the dependence of the total drag coefficient on the Reynolds number. As discussed by Da Costa et al. [5], macroscopic bulk fluid flow through spacers could be arranged in increasing order of "turbulence" (bulk fluid mixing) by analyzing the dependence of the total drag coefficient on the Reynolds number. Simulations in this work showed that spacers could be arranged in the following order in increasing degree of turbulence: NALTEX-56 UF4 NALTEX-51-3 NALTEX-51-1 NALTEX-51-2 NALTEX-124 UF1 NALTEX-129 Conwed-2 Conwed-1.

Based on simulations in this work, in increasing order of total drag coefficient, the spacers could be arranged in the following order: Conwed-2 UF4 UF1 NALTEX-51-3 NALTEX-51-1 NALTEX-56 NALTEX-51-2 NALTEX-124 NALTEX-129 Conwed-1.

Simulations in this work showed that bulk of the fluid flows parallel to the spacer filaments for spacers with equal filament diameter and low inter-filament distance to filament diameter ratios. For example, for Conwed-1 spacer ($_{f}$ $_{f}$ ~ 2) a large proportion of the bulk fluid does not follow a zigzag path, changing direction at each mesh as proposed previously in the literature [5]. CFD simulations showed that a major component of the overall pressure drop was due to the rotation of the velocity vectors across a narrow transition zone corresponding to the plane of intersection of the spacer filament strands. However, for spacers with large inter-filament distance to filament diameter ratios, for example, the NALTEX-56 spacer ($_{f}$ $_{f}$ $\sim$ 8), bulk of the fluid flows parallel to the channel axis. Such insights into the actual fluid flow structure using CFD could be used to design spacers with increased shear and lower total drag.

The main factors influencing design of an effective spacer (high wall shear and low pressure drop) seem to be the ratio of filament diameter to the inter-filament distance, the filament diameter and the angle between the spacer filaments. Filament diameter is an important parameter since it limits the packing density in the final membrane module. The ratio between filament diameter and the inter-filament spacing influences the bulk flow pattern (as discussed above). Each of these cases results in a unique flow field that influences mass transfer.

The order of spacers when arranged in increasing average shear rate was found to be different for high (1 m/s) and low (0.25 m/s) inlet velocities. At 1 m/s inlet velocity, in increasing order of average shear rate, the spacers could be arranged in the following order: UF1 UF4 NALTEX-51-3 NALTEX-129 NALTEX-51-1 NALTEX-56 NALTEX-124 NALTEX-51-2. At 0.25 m/s inlet velocity, this order changed to: UF1 NALTEX-51-3 NALTEX-51-2 NALTEX-124 UF4 NALTEX-129 NALTEX-51-1 NALTEX-56.

Among all the spacers evaluated in this work, NALTEX-51-2 was found to be the most effective spacer in terms of it's relatively low total drag coefficient coupled with a high average shear rate.

It remains to be verified whether the fluid flow across spacer filled channels is in fact "steady". This can be verified by CFD simulations using an appropriate model for turbulence modeling, for example, the RNG–k– model. Such simulations are currently underway and results will be reported in a forthcoming manuscript. Some results have been recently

reported by Cao et al. [9], where they model fluid flow in net-type turbulence promoters as flow past an array of cylinders.

Acknowledgements

The authors are grateful to Dr. Steven Beale and Ron Jerome of the Chemical Systems Analysis Group, ICPET, for providing access to the PHOENICS CFD simulation package.

References

[1] A.R. Da Costa, A.G. Fane, C.J.D. Fell, A.C.M. Franken, Optimal channel spacer design for ultra-filtration, J. Membr. Sci. 62 (1991) 275–291.

[2] W.D. Glatzel, M.C. Tomas, The effect of turbulence promoters on heat transfer and pressure drop in plate heat exchanger, CSIR Special report CHEM 53, 1966.

[3] R.E. Hicks, Chemical engineering group, CSIR Pretoria, South Africa reports CHEM 54, 126 and 138, 1967–1970.

[4] G. Schock, A. Miquel, Mass transfer and pressure loss in spiral-wound modules, Desalination 64 (1987) 339–352.

[5] A.R. Da Costa, A.G. Fane, D.E. Wiley, Spacer characterization and pressure drop modelling in spacer-filled channels for ultra-filtration, J. Membr. Sci. 87 (1994) 79–98.

[6] A.R. Da Costa, A.G. Fane, Net-type spacers: effect of configuration on fluid flow path and ultra-filtration flux, Ind. End. Chem. Res. 33 (1994) 1845–1851.

[7] R.B. Bird, W.E. Stewart, E.R. Lightfoot, Transport Phenomena,